

Group transformations and entangled-state quantum gates with directionally unbiased linear-optical multiports

David S. Simon,^{1,2,*} Casey A. Fitzpatrick,^{2,†} and Alexander V. Sergienko^{2,3,‡}¹*Department of Physics and Astronomy, Stonehill College, 320 Washington Street, Easton, Massachusetts 02357, USA*²*Department of Electrical and Computer Engineering & Photonics Center, Boston University, 8 Saint Mary's Street, Boston, Massachusetts 02215, USA*³*Department of Physics, Boston University, 590 Commonwealth Avenue, Boston, Massachusetts 02215, USA*

(Received 31 October 2015; published 25 April 2016)

The concept of directionally unbiased optical multiports is introduced, in which photons may reflect back out the input direction. A linear-optical implementation is described, and the simplest three-port version studied. Symmetry arguments demonstrate potential for unusual quantum information processing applications. The devices impose group structures on two-photon entangled Bell states and act as universal Bell-state processors to implement probabilistic quantum gates acting on state symmetries. These multiports allow optical scattering experiments to be carried out on arbitrary undirected graphs via linear optics and raise the possibility of linear-optical information processing using group structures formed by optical qudit states.

DOI: [10.1103/PhysRevA.93.043845](https://doi.org/10.1103/PhysRevA.93.043845)

I. INTRODUCTION

Symmetry has long been a guiding principle in physics. Central to linear optics is the beam splitter (BS), which has reflection symmetry as well as a time-reversal symmetry in which a photon may either enter or leave any of the four ports. However, the BS is asymmetric in another sense. Once a photon enters a port, it may not leave from the *same* port: a photon in one port breaks the symmetry. We call this inability to reverse direction *directional bias*. Here we introduce a linear-optical arrangement that restores the symmetry: it is *directionally unbiased*. This arrangement, which can be thought of from multiple viewpoints (as a directionally unbiased multiport BS, as a resonant cavity with three or more exit directions, or as a scattering vertex for an undirected graph), is generalizable to any number of ports $n \geq 3$; we focus on the simplest case of $n = 3$. Despite its simplicity, the high degree of symmetry and the ability of photons to reverse direction lead to interesting properties that allow it to be used as the basis for a variety of applications related to quantum information processing.

Finding practical means of transmitting higher-dimensional optical states (qudits) with a large information capacity is a longstanding goal of quantum communication, but here we raise a further possibility: increasing the number of *operations* that can be applied to qudits and arranging for these operations to form a mathematical group. For example, instead of information processing using a one-dimensional string of N orbital angular momentum states connected in a chain by a single operator and its adjoint, it should be possible to use a set of N states lying on some two (or higher-)dimensional manifold and connected to each other by transformations of some d -dimensional group, so that $N \times d$ parameters are now needed to specify all possible transitions between states. This would allow the power of group theory to be brought to bear

on problems in quantum information processing and quantum communication to a greater degree than it has previously and could potentially offer increased speed and flexibility in areas such as quantum computation [1]. As one example of the new possibilities, consider that group-based quantum cryptography protocols could be constructed in which the qudits being communicated may lie on points of a collection of overlapping sets and in which different sets form representations of different groups. Then, in order to extract information about the key, an eavesdropper might need to obtain not just the *qubits* being sent, but also knowledge of the abstract *group* that joins them and of the *group representation* to which they belong. Group structures have already been shown to be useful for several purposes in classical cryptography [2,3] but have not been widely applied in quantum cryptography protocols.

In the following we show, using only linear optics, that unbiased optical three-ports can encode Bell states [4] in such a way that they form a representation of the Klein Vierergruppe or four-group. Generalized multiports and larger sets of states may allow implementations of larger group representations. We also apply the multiport to an example of processing entangled-photon states, with bits encoded into the state's symmetry. Generalizations and conclusions are then discussed. Elsewhere we will show that networks of unbiased multiports can produce quantum walks with unusual features.

Quantum walks are of great interest for implementing quantum algorithms [5–9]. In Refs. [10–12], quantum walks on graphs were investigated, with scattering at the vertices. Particular attention was paid to an example with three-edge vertices that scatter both backward and forward; in our terminology they are directionally unbiased. The initial motivation for the arrangement presented here was to implement such graphs using only linear optics.

In the current paper, we do not yet make use of the full power of the arrangement presented. In particular, the vertices of the multiport have free parameters (mirror reflectances and phase shifts) that can be varied to produce further effects; but in the present paper we keep all of these parameters fixed and require them to have the same values at all vertices of the multiport. One effect of this is clear: by making the

*simond@bu.edu

†cfitz@bu.edu

‡alexserg@bu.edu

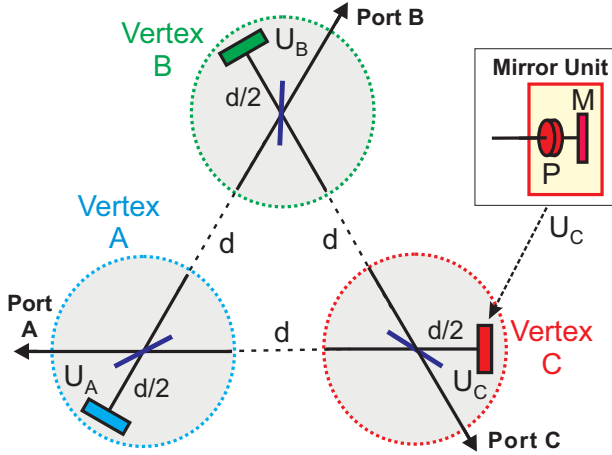


FIG. 1. Schematic of the directionally unbiased three-port. Beam splitters connect input ports to two internal edges and a mirror unit U . U is composed of a mirror M and phase plate P (inset). Reflection at a mirror unit imparts to each photon a total phase factor of $-i$.

vertices identical we are restricting ourselves to Abelian-group structures. By allowing each vertex of the multiport to have different parameter values, it seems likely that non-Abelian structures could be generated as well, although this remains to be investigated in detail.

II. DIRECTIONALLY UNBIASED OPTICAL THREE-PORTS

The arrangement shown in Fig. 1 has three input/output ports, labeled A , B , and C , each attached to two internal edges by a nonpolarizing 50:50 BS ($r = it = \frac{i}{\sqrt{2}}$). Light exiting the remaining port of each BS strikes a mirror normally. Phase plates in front of each mirror add adjustable phase shifts. We keep the phase shift constant at $-\frac{3\pi}{4}$ per passage, so the total phase factor gained at each mirror is $e^{-i\pi/2} = -i$ (including -1 from the mirror itself). This choice makes all exit amplitudes pure imaginary. Beam splitter and mirror losses are neglected.

Assume equal distances d between beam splitters, with BS-to-mirror distance $d/2$. Then $T = \frac{d}{c}$ is the time between successive photon-BS encounters. The probability of not exiting the device decreases exponentially to near zero within several steps (Table I), so for small enough d (such that T is

TABLE I. Amplitudes for paths exiting at time $t = NT$, assuming input at A . Columns 2–4 list the amplitudes for exit at each port. The last two columns list the exit probability at $t = NT$ and the cumulative exit probability at $t \leq NT$.

N	A exit	B exit	C exit	Exit probability	Cumulative exit probability
2	0	$\frac{i}{2}$	$\frac{i}{2}$	$\frac{1}{2}$	0.5
4	$-\frac{i}{2}$	$\frac{i}{4}$	$\frac{i}{4}$	$\frac{3}{8}$	0.875
6	$\frac{i}{4}$	$-\frac{i}{8}$	$-\frac{i}{8}$	$\frac{3}{32}$	0.96875
8	$-\frac{i}{8}$	$\frac{i}{16}$	$\frac{i}{16}$	$\frac{3}{128}$	0.99219
10	$\frac{i}{16}$	$-\frac{i}{32}$	$-\frac{i}{32}$	$\frac{3}{512}$	0.99805

small compared to the photon coherence time) the exit can be treated as instantaneous.

Each photon path through the system has an amplitude of absolute value $2^{-N/2}$, after N BS encounters. The number of paths increases more slowly (roughly linearly) with N , so output states can be calculated to a good approximation from the shortest few paths. For single-photon input at A , summing the amplitudes of all possible paths of length N is straightforward. Amplitudes up to $N = 10$ are tabulated in Appendix A. For $N \geq 3$, the exit probability at the N th step is $3/2^N$ for even N ; the probabilities vanish at odd N .

Ignoring overall normalization, the resulting state is $|\psi(t)\rangle = a(t)|A\rangle + b(t)(|B\rangle + |C\rangle) + |\psi_{\text{int}}(t)\rangle$, where

$$a(t) = \left(-\frac{i}{2}\Theta(t-4T) + \frac{i}{4}\Theta(t-6T) - \frac{i}{8}\Theta(t-8T) + \frac{i}{16}\Theta(t-10T) \right) + O(2^{-5}), \quad (1)$$

$$b(t) = \left(\frac{i}{2}\Theta(t-2T) + \frac{i}{4}\Theta(t-4T) - \frac{i}{8}\Theta(t-6T) + \frac{i}{16}\Theta(t-8T) - \frac{i}{32}\Theta(t-10T) \right) + O(2^{-6}). \quad (2)$$

$|A\rangle$, $|B\rangle$, and $|C\rangle$ are shorthand for single-photon states $|1\rangle_A|0\rangle_B|0\rangle_C$, $|0\rangle_A|1\rangle_B|0\rangle_C$, and $|0\rangle_A|0\rangle_B|1\rangle_C$. The step function $\Theta(t)$ vanishes for $t < 0$ and equals unity for $t > 0$. Finally, $|\psi_{\text{int}}(t)\rangle$ is the state with the photon still inside the device; its exponentially decaying amplitude can also be obtained by summation of paths.

The transient internal state $|\psi_{\text{int}}(t)\rangle$ decays with characteristic time taken conservatively as $T_c \approx 10T$. If the detector response time T_D exceeds T_c , the possible photon paths are indistinguishable, so the exit state is a coherent superposition of outputs at different ports. Integrated onto a chip, d could be very small; as a conservative example take $d = 0.1$ mm. Then $T_c = 3.3$ ps, allowing sampling at rates up to 0.3 THz. Using a tabletop setup, d would be of the order of centimeters, with a proportionally lower maximum sampling rate.

For information processing, timing information must be supplied to synchronize gates. For instance, a CW source can be gated to form pulses. Assuming a Gaussian temporal envelope, the pulse duration Δt and spectral width $\Delta\nu$ are related by $\Delta t \Delta\nu = \frac{1}{4\pi}$ [13]. For example, pulses of $\Delta t \sim 10^{-10}$ s have $\Delta\nu \sim 1$ GHz, giving a coherence time and length of $\tau_{\text{coh}} = \frac{1}{\Delta\nu} \approx 1$ ns and $l_{\text{coh}} \approx 30$ cm, consistent with the constraints above. Using parametric down conversion is another possibility, with the signal sent into the multiport and the idler heralding the event to provide timing information. In this case, signal coherence times are of the order $\tau_{\text{coh}} \sim 1$ ps, leading to coherence length $l_{\text{coh}} \sim 10^{-4}$ m, bordering on the acceptable limit in the example above.

If the unit is constructed on a chip, then the refractive index of the chip will increase the transit time T (by a factor of 2–4 for materials like silicon nitride and silicon). This will tighten the constraints somewhat. Using the numbers above, this would rule out parametric down conversion, but it still leaves the gated CW source as a plausible possibility, with a correspondingly reduced sampling rate.

Before treating the three-port quantitatively, let us look at some potential problems that could arise. First, when $T_D < T_c$, different exit times for the same input become distinguishable. In this case, the output will be a mixed state, and the system behaves classically. Further, when the wave packet has a finite coherence time, the corresponding frequency spread in the packet will cause different parts of the packet to go out of phase with each other, introducing a phase spread of up to $\Delta\phi = d \Delta k = \frac{2\pi d}{c\tau_{\text{coh}}}$ during propagation along each edge. This will affect the shape of the wave packet through interference, as well as introducing some spectral dependence into the output. All of these troublesome effects are to be avoided for high-quality output, so keeping their effects at a minimal level is necessary to make sure that the inequalities $\tau_{\text{coh}} \gg T_D > T_c$ hold.

A further potential problem is that when the multiport is used as a vertex in a quantum walk, the number of steps over which the walk will retain its quantum nature will be limited because of the broadening of wave packets that results from the existence of different-length paths through the multiport. The maximum number of steps possible for the quantum walk will then be given roughly by the ratio τ_{coh}/T_c ; this again highlights the importance of maintaining the inequalities given above. By the same reasoning, when the multiport is used as a quantum gate the number of such gates that can be connected in sequence will be limited by the same ratio. For the examples given above, it can be seen that the gated laser pulse should be able, under ideal conditions, to maintain a quantum walk for dozens of steps, while the down-conversion example will not be able to support walks of more than a couple of steps.

Given the considerations above, we now assume that $\tau_{\text{coh}} \gg T_D > T_c$. Then the input $|\psi_{\text{in}}\rangle = |A\rangle$ leads to

$$|\psi_{\text{out}}\rangle \approx -i\left(\frac{1}{2} - \frac{1}{4} + \frac{1}{8} - \frac{1}{16}\right)|A\rangle + i\left(\frac{1}{2} + \frac{1}{4} - \frac{1}{8} + \frac{1}{16} - \frac{1}{32}\right)(|B\rangle + |C\rangle). \quad (3)$$

The $A \rightarrow A$ part gives the first few terms in a geometric series. Assuming that this pattern continues, the $A \rightarrow A$ transition amplitude is therefore

$$-\frac{i}{2} \sum_{n=0}^{\infty} \left(-\frac{1}{2}\right)^n = -\frac{i}{2} \left(\frac{1}{1+1/2}\right) = -\frac{i}{3}. \quad (4)$$

By similar extrapolation, the $A \rightarrow B$ and $A \rightarrow C$ coefficients are both

$$i \left[\frac{1}{2} + \frac{1}{4} \sum_{n=0}^{\infty} \left(-\frac{1}{2}\right)^n \right] = i \left(\frac{1}{2} + \frac{1}{6} \right) = \frac{2}{3}i. \quad (5)$$

Rotational symmetry allows transition amplitudes for input at other ports to be obtained by cyclic permutation, giving the long-time single-photon unitary transition matrix: $U|\psi_{\text{out}}\rangle = U|\psi_{\text{in}}\rangle$, where (in the $|A\rangle, |B\rangle, |C\rangle$ basis)

$$U = -\frac{i}{3} \begin{pmatrix} 1 & -2 & -2 \\ -2 & 1 & -2 \\ -2 & -2 & 1 \end{pmatrix}. \quad (6)$$

Up to an overall phase, U gives the reflection and transmission amplitudes from [10–12].

This matrix can also be found from more general unitarity and symmetry arguments, as follows. Assume that a photon is sent into port A . Due to reflection symmetry about the input direction, the exit amplitudes at the other two ports should be equal. Therefore, for $|\psi_{\text{in}}\rangle = |A\rangle$, the output must be of the form

$$|\psi_{\text{out}}\rangle = a|A\rangle + b(|B\rangle + |C\rangle) \quad (7)$$

for complex amplitudes a and b . Repeating the argument for inputs at ports B and C , the system's transition matrix V must be of the form

$$V = \begin{pmatrix} a & b & b \\ b & a & b \\ b & b & a \end{pmatrix}. \quad (8)$$

The matrix must be unitary, so that $V \cdot V^\dagger = I$; the diagonal and off-diagonal entries of this condition imply two constraints:

$$|a|^2 + 2|b|^2 = 1, \quad 2\text{Re}(ab^*) + |b|^2 = 0. \quad (9)$$

Defining $a = \alpha e^{i\phi_a}$, $b = \beta e^{i\phi_b}$, and $\phi = \phi_b - \phi_a$, then solving these unitarity constraints gives

$$\alpha = \sqrt{\frac{1}{1+8\cos^2\phi}}, \quad \beta = -2\sqrt{\frac{\cos^2\phi}{1+8\cos^2\phi}}. \quad (10)$$

So the most general form of V is

$$V = \frac{e^{i\phi_a}}{\sqrt{1+8\cos^2\phi}} \begin{pmatrix} 1 & -2\cos\phi & -2\cos\phi \\ -2\cos\phi & 1 & -2\cos\phi \\ -2\cos\phi & -2\cos\phi & 1 \end{pmatrix}. \quad (11)$$

In the special case where $\phi = 0$, this becomes

$$V(\phi_a) = \frac{1}{3} e^{i\phi_a} \begin{pmatrix} 1 & -2 & -2 \\ -2 & 1 & -2 \\ -2 & -2 & 1 \end{pmatrix}. \quad (12)$$

For $\phi_a = -\frac{\pi}{2}$ this gives back the matrix U of Eq. (6).

It should be pointed out that, up to an overall phase, Eq. (6) is the same as the well-known Grover coin for three-dimensional coined quantum walks. Similarly, the unbiased n -ports with $n > 3$ that are discussed briefly in Sec. VI correspond, when appropriate choices are made for the phases at the mirrors, to higher-dimensional Grover coins. Therefore, the unbiased n -ports can also be viewed as particularly simple linear-optical realizations of n -dimensional Grover coins. Note, however, that the unbiased n -ports are more general than this: by changing the phases and reflectances other coins can be implemented as well.

III. ACTION ON BELL STATES

For two-photon entangled states, coherence requirements are less stringent than for single-photon states, since it is primarily the much longer coherence time of the pump that is relevant, rather than the coherence times of the signal and idler. Further, spectral filtering can stretch out the coherence time and remove distinguishability due to the arrival time within each pair [14]. So it is natural to consider the action on two-photon states. Advantage can be taken of this in order to

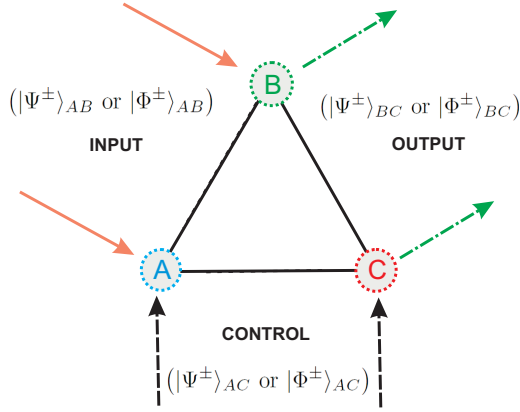


FIG. 2. Two-photon input enters ports A/B , with the control state entering A/C . Output exits ports B/C .

construct quantum gates in which the input and output qubits are not defined by identities of individual photons but, rather, by the symmetries shared by pairs of ingoing and outgoing two-photon states.

Applying appropriate control states, the multiport can convert any input Bell state into any output Bell state. The states considered here are distributed over two ports, for example, $|\Psi^\pm\rangle_{AB} = \frac{1}{\sqrt{2}}(|H\rangle_A|V\rangle_B \pm |V\rangle_A|H\rangle_B)$ and $|\Phi^\pm\rangle_{AB} = \frac{1}{\sqrt{2}}(|H\rangle_A|H\rangle_B \pm |V\rangle_A|V\rangle_B)$ at A and B . H and V denote horizontal and vertical polarization. Similar states are defined at other pairs of ports. Although mirror units interchange horizontal and vertical polarizations, every path through the system encounters an even number of such units, leaving polarizations unchanged.

Consider creating two Bell states (by the procedure used in [14], for example): a target state and a control state (Fig. 2). These are input at ports AB (input) and AC (control). They are coupled into fibers, and the portions being fed into the same port are merged using integrated Y couplers. The output, which can be separated from the input by an optical circulator, will be an entangled state shared by B and C . Consider states with one photon exiting at B and one at C . (If multiple gates are concatenated, states with two photons exiting the same port need to be rejected. Methods for doing this are known [15]). There will then be two photons exiting A . Acceptance of BC output states is conditioned upon some outcome at A . The choice of conditioning outcome provides control over the gate action. Consider two possibilities: conditioned upon detecting two photons of either opposite polarization (o) or same polarization (s) at A . It is necessary only to determine whether or not the polarizations are the same, not to determine what the polarizations are (similar to the probabilistic gates in [16–19]).

Computing outputs for any input and control, and for either heralding condition, is straightforward (sample calculations are given in Appendix B) and result in Table II. We see that the multiport acts as a universal processor on Bell states; with the appropriate choice of control and heralding conditions any input state can be converted to any desired output state.

TABLE II. Action on Bell states. The input is at AB , and the control at AC , with the output at BC conditioned, respectively, on detecting the same (s) or opposite (o) polarizations at A .

Input	Control	Output		Input	Control	Output	
		s	o			s	o
Ψ^+	Ψ^+	Φ^+	Ψ^+	Ψ^+	Φ^+	Ψ^+	Φ^+
Ψ^+	Ψ^-	Φ^-	Ψ^-	Ψ^+	Φ^-	Ψ^-	Φ^-
Ψ^-	Ψ^+	Φ^-	Ψ^-	Ψ^-	Φ^+	Ψ^-	Φ^-
Ψ^-	Ψ^-	Φ^+	Ψ^+	Ψ^-	Φ^-	Ψ^+	Φ^+
Φ^+	Φ^+	Φ^+	Ψ^+	Φ^+	Ψ^+	Ψ^+	Φ^+
Φ^+	Φ^-	Φ^-	Ψ^-	Φ^+	Ψ^-	Ψ^-	Φ^-
Φ^-	Φ^+	Φ^-	Ψ^-	Φ^-	Ψ^+	Ψ^-	Φ^-
Φ^-	Φ^-	Φ^+	Ψ^+	Φ^-	Ψ^-	Ψ^+	Φ^+

IV. PROBABILISTIC CONTROLLED ENTANGLED-STATE GATES

Taking subsets of Table II, we may implement probabilistic quantum gates. For example, take $|\Psi^+\rangle_{AB}$ as input. Table III shows how, by varying just the control state and holding the heralding condition fixed, any desired state can be selected from the possible output states. The same can be done using any other Bell input state.

As one example of symmetry-based Bell-state processing, the multiport implements probabilistic CNOT gates for entangled states. Take $|\Psi^\pm\rangle$ states as input and control, but $|\Phi^\pm\rangle$ states as output, with positive states of either type corresponding to $|0\rangle$ and negative states to $|1\rangle$ in all cases. (So the bit is determined by the polarization-interchange symmetry, not by the particular state that happens to be carrying the symmetry.) Attention is then restricted to the top-left quadrant in Table II under condition s , yielding a CNOT truth table. For multiple processing steps through multiple gates, the roles of $|\Psi^\pm\rangle$ and $|\Phi^\pm\rangle$ flip in alternate clock steps: output $|\Phi^\pm\rangle$ states at one step will become input for the next step, with $|\Psi^\pm\rangle$ states then being output at that next step. In alternate steps, the bottom-left quadrant in Table II would be used. The success probability for this *four-photon* gate is about 5%, not far below the lower end of the success probability range for the proposed *two-photon* probabilistic gates ($\sim \frac{1}{6}$ to $\frac{1}{2}$) [16–22]. Instead of encoding qubits into the state symmetry, the Bell states can also be viewed as qudits in a four-dimensional Hilbert space. The multiport then would act as a four-photon, *two-qudit* gate.

TABLE III. Ψ^+ can be converted to any desired output Bell state. Here the s condition is assumed.

Input	Control state	Output
Ψ^+	Ψ^+	Φ^+
Ψ^+	Ψ^-	Φ^-
Ψ^+	Φ^+	Ψ^+
Ψ^+	Φ^-	Ψ^-

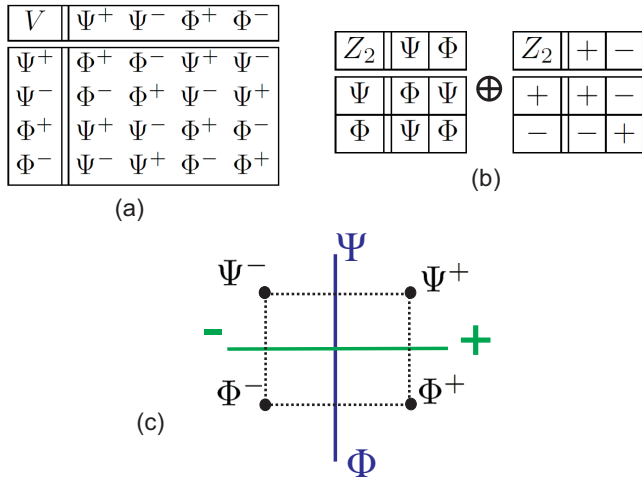


FIG. 3. (a) The multipoint produces the Abelian four-group multiplication table. (b) Cyclic Z_2 subgroups describe reflections about axes shown in (c).

V. GROUP STRUCTURE

The device turns two ingoing states into one output state. When the s condition is used, this imposes an Abelian-group structure on the states. (For the o condition, the same structure appears, with $|\Phi^\pm\rangle$ and $|\Psi^\pm\rangle$ interchanged.) The resulting group multiplication table in Fig. 3(a) has rows and columns labeling input and control states; output occupies the interior. This is the Klein four-group [23], V , which is a direct sum of two cyclic groups, $V = Z_2 \oplus Z_2$ [Fig. 3(b)]. The action of this group is not difficult to understand: consider the two-dimensional space with one axis labeled $+$ and $-$ (right and left) and the other Ψ and Φ (up and down). Bell states are then at corners of a rectangle, and the Z_2 groups reflect the axes [Fig. 3(c)]. If input states are restricted to $\{|\Psi^+\rangle, |\Phi^+\rangle\}$, then a single Z_2 group arises.

This raises interesting possibilities. Postselection introduces effective “interactions” between photons with states acting on each other via mathematical groups. The triangular device is suited for this, with two sides to use for the input of the two ingoing states and the third side for the group product output. Because all vertices are taken to be identical, it is clear that only Abelian groups can occur here: interchanging which state enters which side can have no effect on the outcome. However, when using different complex reflectances at different vertices, the symmetry of the device is broken; as a result, changing the order of multiplication of the states (which state is applied to which side of the triangle) will now affect the outcome. In the latter case any groups that arise would be expected to be non-Abelian. In addition, it remains to be investigated whether larger groups could be obtained from larger sets of input states and from multipoints with more than three vertices. In any case, the ability to engineer groups of states opens new avenues of investigation of optically implemented group representations for quantum information processing, such as group-based strategies for quantum cryptography or group-based security mechanisms for quantum key distribution.

As one example of why a group approach may be useful, consider information processing with d -state logic. Imagine that possible input and output states form a faithful representation in Hilbert space of a group G of order d . The full range of operations possible in this set of states (the transformation of any of the d inputs to any of the d outputs) would require a total of d operations. But suppose that the group is of rank r , with a set of generators g_1, \dots, g_r . This means that any element $g \in G$ can be written in the form $g = g_1^{n_1} \cdot g_2^{n_2} \cdot \dots \cdot g_r^{n_r}$ for some appropriate set of integers n_1, \dots, n_r . This is the case for the Klein group, for example, where the four-element group is generated by the two generators of the Z_2 subgroups. Similarly, a set of states lying in a plane and related by a discrete rotation group of any rank can always be spanned by powers of just a single generator. Therefore d -state logic can be carried out in a group representation in Hilbert space with only r types of basic logic units. In the directionally unbiased scheme presented here, different logic units would correspond to triangular (or more general polygonal) units with the vertex parameters possibly set to different values or with different control states. In the case where r is much smaller than d , then very high-order logic systems can be implemented with a small number of different logic units. This increased parsimony is illustrated by the construction in Secs. III and IV, where four different operations on a given target state are carried out by a single triangular controlled logic unit.

As mentioned in Sec. I, new possibilities may be raised for quantum cryptographic schemes as well. For example, there is also a connection between the approach in this paper and a group-theory-related quantum key distribution protocol that has already been proposed. This is the quantum enigma scheme [24,25], which is based on quantum data locking: a small amount of transmitted information can unlock a much larger trove of data to a user, while keeping the data secure from unapproved agents. This is done by using a set of $N \times N$ unitary matrices [i.e., elements of the group $U(N)$] to rotate between a collection of mutually unbiased bases. A randomly chosen element in this set is applied to an initial state. An eavesdropper cannot access the information in the transmitted state without knowing what unitary transformation is needed to rotate it back to its original basis. Rather than sending the entire unitary matrix, only a discrete label identifying the matrix needs to be securely transmitted. The approach in the current paper constructs discrete group transformations, which can be embedded into the continuous groups $U(N)$ and, so, can be viewed as a physical implementation of the quantum enigma transformations for low N . Returning to the example of the Klein group, the four Bell states are related by a discrete subgroup of the unitary group $U(2)$ acting on the two-dimensional complex space spanned by the basis $|H\rangle$ and $|V\rangle$. To be useful for the enigma procedure, the current setup must be generalized by using more complex input and output states, in order to allow larger subsets of higher $U(N)$ groups to appear.

VI. GENERALIZATIONS AND FURTHER DIRECTIONS

The triangular geometry can be replaced by any regular n -sided polygon, such as the four-port in Fig. 4. This enlarges the symmetry group of the device and allows the imposition of

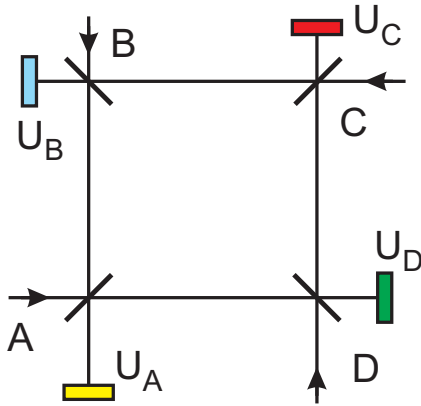


FIG. 4. Directionally unbiased four-port. Generalizations to any number of ports ≥ 3 are possible.

other, more complex group structures on the input and output states. This will, in turn, expand the potential capacity for information processing applications. Using arbitrary polygonal units allows the implementation of scattering experiments on undirected graphs with nodes of arbitrary valence.

For n -ports with $n > 3$, if d is not an integer multiple of the wavelength, then paths between ports separated by different distances will gain different phase shifts and different amplitude losses (due to the different numbers of intervening beam splitters crossed). The phase shifts can cause possible interference effects within the multiport. As a result, the off-diagonal terms in U are no longer all equal. This effect will be unavoidable for finite pulses with a nonzero frequency spread. However, if d is an integer multiple of the central wavelength of the pulse, then the effect will again be small if the coherence time is long or, in other words, if the spread of wavelengths away from the central value is small. Even for long τ_{coh} this will eventually become significant if the multiport is made sufficiently large [in the sense of having a large number of input (output) ports], but if the details of the pulse are known, then the effect on U can be calculated. The overall symmetries of the multiport under reflection and rotation will still be maintained, but the output will depend on the distance between the input and the output ports, as reflected by the change in the off-diagonal entries in U .

In this paper a single triangular unit has been considered in isolation. When they are connected in networks, new possibilities arise. For example, quantum walks on lattices with different symmetries and with vertices having easily controllable properties can be constructed in a simple manner. The fact that all of the elements of the basic polygonal multiport can be put onto a single optical chip means that large networks can be readily constructed, with fewer alignment and stability problems than would occur using tabletop arrangements of discrete beam splitters and mirrors. Different polygons can be joined together in the same network (for example, triangular, square, and pentagonal multiports) in order to experimentally study more complex systems or behavioral changes in the system due to transition from one symmetry type to another. Scattering systems in undirected graphs can then be studied experimentally, including graphs with different valences at different nodes.

Variation of the system's parameters can also be introduced. Reflectances and mirror unit phase shifts may differ at each corner, allowing tailoring of a range of output qutrits from the same input state by parameter tuning. In two-dimensional networks of such units, this parameter tuning allows the introduction of controlled spatial bias into quantum walks, which is useful for algorithmic applications [26]. Further, parameters can be varied while a walk is in progress, allowing investigations of time-dependent quantum walks.

VII. CONCLUSIONS

In this paper, linear-optical unbiased multiports have been introduced. Symmetry arguments and path tracing show that, despite its simplicity, this system has a number of unusual properties and applications. These devices allow simple implementations of optical scattering experiments on graphs, information processing directly in Bell states or other more complicated state sets, and information processing in optically implemented group structures. Some tentative possible directions have been raised for applications of a group-based approach to optical cryptography and information processing.

It should also be noted that the current directionally unbiased framework differs in several important ways from all linear-optical information processing schemes that fall into the Knill-Laflamme-Milburn (KLM) [20] framework. For example, KLM-based schemes always consider only output states with at most a single photon in each output mode. Those output states with multiple photons in the same mode are considered to be signals that the desired operation has failed, and so they are discarded. In contrast, in the scheme described in this paper constructive use is made of the possibility that multiple photons may leave the device in the same mode. Similarly, in KLM-type setups, the input and output ports are always distinct from each other, with the photons always traveling in a single direction through the network. The introduction of directionally unbiased propagation in our scheme allows the merging of input and output ports, which can greatly decrease the complexity of an optical network; for example, the number of beam splitters in general scales quadratically in N for KLM networks, where N is the number of photons or, equivalently, the number of input or output ports. In the present case, the unbiased N -port setup can process N photons through N input or output ports with just N beam splitters and N mirrors; it therefore scales only linearly with N . For large N , this drop in scaling from quadratic to linear is an enormous savings of resources.

A rich range of further possibilities remains to be explored, such as optical implementation of three-state logic using qutrits on triangular multiports or of higher-state logic on larger polygonal multiports.

ACKNOWLEDGMENTS

This research was supported by the DARPA QUINESS program through US Army Research Office award W31P4Q-12-1-0015, by the National Science Foundation under Grant No. ECCS-1309209, and by Northrop Grumman Aerospace Systems.

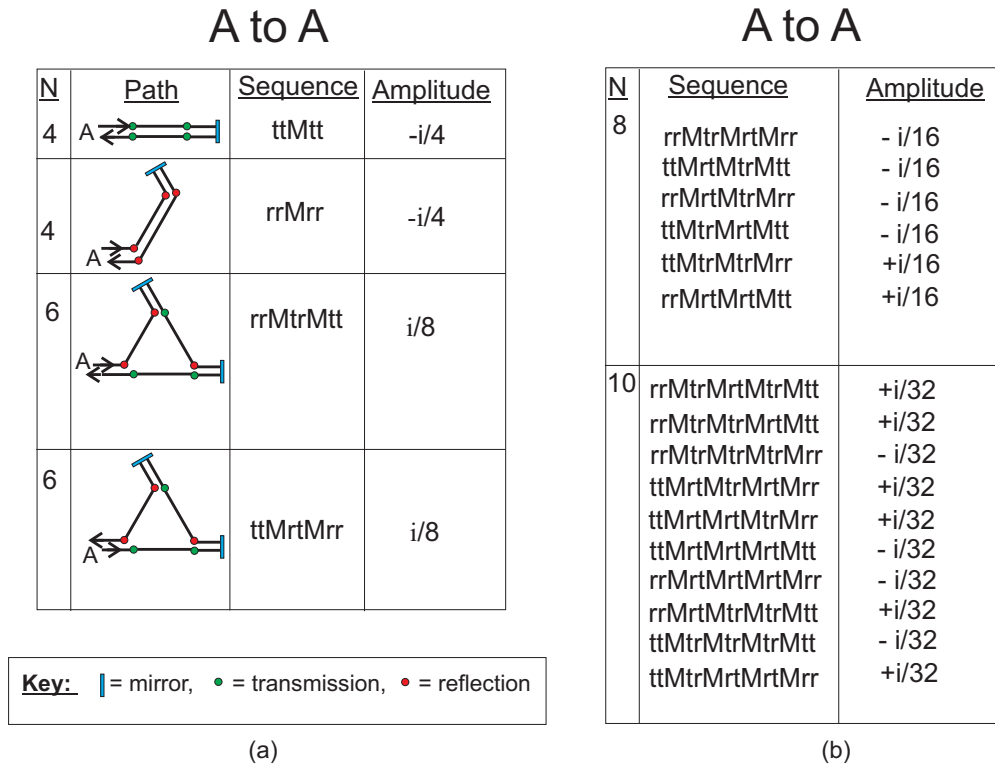


FIG. 5. Paths of length up to $N = 10$ that enter port A and then exit at the same port.

APPENDIX A: PATHS AND AMPLITUDES THROUGH THE DEVICE

Here, the paths of length $N \leq 10$ that start at A and exit the system are tabulated, along with their amplitudes. A few

other properties of the transition matrix U are also given, for completeness.

The possible paths are given in the tables in Figs. 5–7. In each line, the path is given in symbolic form, with r , t , and M , respectively, representing reflection or transmission at a

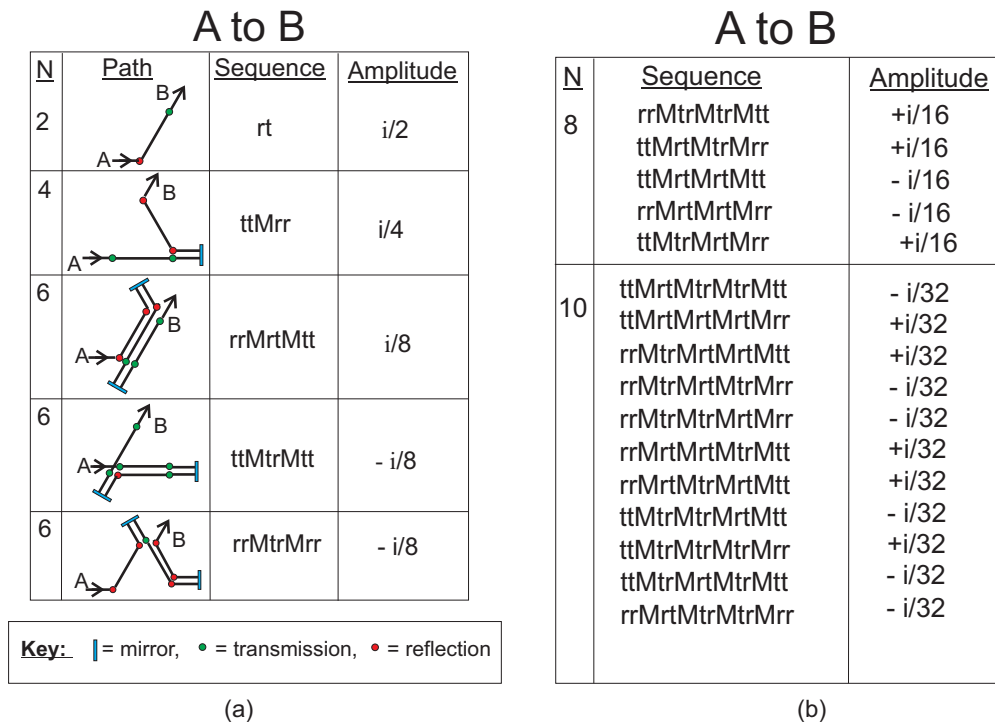


FIG. 6. Paths of length up to $N = 10$ that enter port A and then exit at port B .

A to C				A to C		
N	Path	Sequence	Amplitude	N	Sequence	Amplitude
2		tr	$i/2$	8	rrMtrMrtMtt	$+i/16$
4		rrMtt	$i/4$		rrMtrMtrMrr	$+i/16$
6		ttMtrMrr	$i/8$		ttMrtMrtMrr	$-i/16$
6		rrMrtMrr	$-i/8$		rrMrtMtrMtt	$-i/16$
6		ttMrtMtt	$-i/8$		ttMtrMtrMtt	$+i/16$
Key: = mirror, = transmission, = reflection				10	rrMtrMrtMrtMrr	$-i/32$
					rrMtrMtrMtrMtt	$+i/32$
					ttMrtMtrMtrMrr	$+i/32$
					ttMrtMrtMrtMtt	$-i/32$
					ttMrtMrtMtrMtt	$-i/32$
					ttMtrMtrMrtMrr	$+i/32$
					ttMtrMrtMtrMrr	$+i/32$
					rrMrtMrtMtrMrr	$-i/32$
					rrMrtMrtMrtMtt	$+i/32$
					rrMrtMtrMrtMrr	$-i/32$
				ttMtrMrtMrtMtt	$-i/32$	

FIG. 7. Paths of length up to $N = 8$ that enter port A and then exit at port C .

beam splitter and reflection at a mirror. Drawings of the paths after $N = 6$ are not included because they start becoming too cumbersome. The sequences of reflections and transmissions are ordered from left (first one applied) to right (last). Although it is assumed that the input is at A , there is no loss of generality: the paths for input at the other ports can immediately be obtained from these by cyclic permutation. We assume 50:50 beam splitters, with factors of i for BS reflections and a total reflection coefficient $-i$ at each mirror unit.

Summing the entire infinite series of paths leads to the transition matrix U given in the text. U has one eigenvector with eigenvalue $+i$, given by

$$\frac{1}{\sqrt{3}} \begin{pmatrix} 1 \\ 1 \\ 1 \end{pmatrix} = \frac{1}{\sqrt{3}}(|A\rangle + |B\rangle + |C\rangle), \quad (\text{A1})$$

where $|A\rangle$, $|B\rangle$, and $|C\rangle$ are defined in the text. The remaining two eigenvectors are degenerate, with eigenvalue $-i$, and may be taken to be any two of the three linearly dependent vectors

$$\frac{1}{\sqrt{2}} \begin{pmatrix} 1 \\ -1 \\ 0 \end{pmatrix} = \frac{1}{\sqrt{2}}(|A\rangle - |B\rangle), \quad (\text{A2})$$

$$\frac{1}{\sqrt{2}} \begin{pmatrix} 1 \\ 0 \\ -1 \end{pmatrix} = \frac{1}{\sqrt{2}}(|A\rangle - |C\rangle), \quad (\text{A3})$$

$$\frac{1}{\sqrt{2}} \begin{pmatrix} 0 \\ 1 \\ -1 \end{pmatrix} = \frac{1}{\sqrt{2}}(|B\rangle - |C\rangle). \quad (\text{A4})$$

The eigenstates are therefore those that are either antisymmetric about any pair of ports or completely symmetric about all

three ports. It may also be noted that $U^2 = -I$, where I is the 3×3 identity matrix.

The probability of exiting at a given time is given by adding the amplitudes of the indistinguishable paths that exit at the same port, then adding the probabilities of the different ports. For even N ($N > 2$), the instantaneous exit probability at time $t = NT$ is $6/N^2$, so that the cumulative probability of exiting by time NT is

$$\frac{1}{2} + \frac{3}{2} \sum_{n=2}^{N/2} \frac{1}{n^2}.$$

Exit probabilities at odd N vanish.

APPENDIX B: SAMPLE CALCULATION FOR PROCESSING OF BELL STATES

Here, an example is given of the calculations done to compile Table II. Suppose that the input state is $|\Psi^+\rangle_{AB}$ and the control state is $|\Psi^+\rangle_{AC}$. Then the action of the multiport is

$$|\Psi^+\rangle_{AB} \otimes |\Psi^+\rangle_{AC} \rightarrow (U \otimes U)|\Psi^+\rangle_{AB} \otimes (U \otimes U)|\Psi^+\rangle_{AC}, \quad (\text{B1})$$

where a few lines of algebra starting from Eqs. (5) and (6) in the text give

$$\begin{aligned} (U \otimes U)|\Psi^+\rangle_{AB} \\ = -\frac{1}{9}\{2\sqrt{2}(|H\rangle_A|V\rangle_A + |H\rangle_B|V\rangle_B - 2|H\rangle_C|V\rangle_C) \\ - 5|\Psi^+\rangle_{AB} - 2(|\Psi^+\rangle_{AC} + |\Psi^+\rangle_{BC})\}, \quad (\text{B2}) \end{aligned}$$

with a similar result for $U|\Psi^+\rangle_{AB}$. Taking the product $(U \otimes U|\Psi^+\rangle_{AB}) \otimes (U \otimes U|\Psi^+\rangle_{AC})$ gives

$$\frac{1}{81}\{-8\sqrt{2}|H\rangle_A|V\rangle_A|\Psi^+\rangle_{BC} + 29|\Psi^+\rangle_{AC}|\Psi^+\rangle_{AB} + \dots\}, \quad (\text{B3})$$

where the dropped terms are those that do *not* have a single photon at B and a single photon at C . Note that

$$\begin{aligned} |\Psi^+\rangle_{AB}|\Psi^+\rangle_{AC} = & \frac{1}{2}\{\sqrt{2}|2H\rangle_A|V\rangle_B|V\rangle_C \\ & + \sqrt{2}|2V\rangle_A|H\rangle_B|H\rangle_C \\ & + |H\rangle_A|V\rangle_A(|V\rangle_B|H\rangle_C + |H\rangle_B|V\rangle_C)\}, \end{aligned} \quad (\text{B4})$$

where, for example, $|2H\rangle_A$ is the state with two horizontally polarized photons at A . Using this, the outgoing state becomes

$$\frac{1}{81}\left\{13\sqrt{2}|H\rangle_A|V\rangle_A|\Psi^+\rangle_{BC} + \frac{29}{\sqrt{2}}[|2H\rangle_A|V\rangle_B|V\rangle_C + |2V\rangle_A|H\rangle_B|H\rangle_C] + \dots\right\}. \quad (\text{B5})$$

By projecting onto the part with opposite polarizations at A (the first term), the state $|\Psi^+\rangle_{BC}$ is picked out, while projecting onto the portion with the same polarizations at A (second and third terms) picks out the state

$$\frac{1}{\sqrt{2}}[|V\rangle_B|V\rangle_C + |H\rangle_B|H\rangle_C] = |\Psi^+\rangle_{BC}. \quad (\text{B6})$$

Repeating the same procedure for all possible products of input and control states then fills out the entries in Table II.

-
- [1] G. Falci and E. Paladino, *Int. J. Quantum. Info.* **12**, 1430003 (2014).
- [2] S. R. Blackburn, C. Carlos, and C. Mullan, in *Groups St. Andrews 2009 in Bath*, edited by C. M. Campbell *et al.* (Cambridge University Press, Cambridge, UK, 2011), pp. 133–149.
- [3] M. I. González Vasco and R. Steinwandt, *Group Theoretic Cryptography* (Chapman and Hall/CRC, Boca Raton, FL, 2015).
- [4] M. Genovese, *Phys. Rep.* **413**, 319 (2005).
- [5] Y. Aharonov, L. Davidovich, and N. Zagury, *Phys. Rev. A* **48**, 1687 (1993).
- [6] J. Kempe, *Contemp. Phys.* **44**, 307 (2003).
- [7] S. E. Venegas-Andraca, *Quant. Info. Proc.* **11**, 1015 (2012).
- [8] R. Portugal, *Quantum Walks and Search Algorithms* (Springer, Berlin, 2013).
- [9] A. M. Childs, *Phys. Rev. Lett.* **102**, 180501 (2009).
- [10] E. Feldman and M. Hillery, *Phys. Lett. A* **324**, 277 (2004).
- [11] E. Feldman and M. Hillery, *Contemp. Math.* **381**, 71 (2005).
- [12] E. Feldman and M. Hillery, *J. Phys. A: Math. Theor.* **40**, 11343 (2007).
- [13] B. E. A. Saleh and M. C. Teich, *Fundamentals of Photonics*, 2nd ed. (Wiley-Interscience, Hoboken, NJ, 2007).
- [14] J. W. Pan, M. Daniell, S. Gasparoni, G. Weihs, and A. Zeilinger, *Phys. Rev. Lett.* **86**, 4435 (2001).
- [15] S. D. Barrett, P. Kok, K. Nemoto, R. G. Beausoleil, W. J. Munro, and T. P. Spiller, *Phys. Rev. A* **71**, 060302(R) (2005).
- [16] T. B. Pittman, B. C. Jacobs, and J. D. Franson, *Phys. Rev. A* **64**, 062311 (2001).
- [17] T. B. Pittman, B. C. Jacobs, and J. D. Franson, *Phys. Rev. Lett.* **88**, 257902 (2002).
- [18] T. B. Pittman, M. J. Fitch, B. C. Jacobs, and J. D. Franson, *Phys. Rev. A* **68**, 032316 (2003).
- [19] T. B. Pittman, B. C. Jacobs, and J. D. Franson, *Phys. Rev. A* **71**, 032307 (2005).
- [20] E. Knill, R. Laflamme, and G. J. Milburn, *Nature (London)* **409**, 46 (2001).
- [21] M. Koashi, T. Yamamoto, and N. Imoto, *Phys. Rev. A* **63**, 030301 (2001).
- [22] D. B. Uskov, P. M. Alsing, M. L. Fanto, L. Kaplan, and A. M. Smith, [arXiv:1306.4062](https://arxiv.org/abs/1306.4062) [quant-ph].
- [23] M. A. Armstrong, *Groups and Symmetry* (Springer, Berlin, 1988).
- [24] S. Lloyd, [arXiv:1307.0380](https://arxiv.org/abs/1307.0380).
- [25] S. Guha, P. Hayden, H. Krovi, S. Lloyd, C. Lupo, J. H. Shapiro, M. Takeoka, and M. M. Wilde, *Phys. Rev. X* **4**, 011016 (2014).
- [26] D. Lu, J. D. Biamonte, J. Li, H. Li, T. H. Johnson, V. Bergholm, M. Faccin, Z. Zimborás, R. Laflamme, J. Baugh, and S. Lloyd, *Phys. Rev. A* **93**, 042302 (2016).